Atomically resolved imaging of a CaF bilayer on Si(111): Subsurface atoms and the image contrast in scanning force microscopy

Andreas Klust,[1,*] Taisuke Ohta,[2] Aaron A. Bostwick,[1] Qiuming Yu,[1] Fumio S. Ohuchi,[2] and Marjorie A. Olmstead[1]
[1]*Department of Physics, University of Washington, Box 351560, Seattle, Washington 98195-1560, USA*
[2]*Department of Materials Science and Engineering, University of Washington, Box 352120, Seattle, Washington 98195-2120, USA*
(Received 9 October 2003; published 12 January 2004)

The CaF bilayer on Si(111) was imaged with atomic resolution scanning force microscopy (SFM). The CaF bilayer has almost exactly the same geometry as the uppermost two atomic layers of bulk CaF_2; the positions of the F atoms below the Ca layer, however, are vacant. We discuss the influence of this difference on atomic scale contrast formation in SFM. The SFM images obtained on the CaF bilayer are very similar to results from the literature obtained on bulk CaF_2 with positively terminated tips. SFM observations on the CaF bilayer are explained within a model based on the electrostatic and van der Waals forces between tip and sample. The model predicts that the atomic corrugation is independent of the charge located at the position of the F vacancies and thus explains the similarity of SFM images obtained on bulk CaF_2 and the CaF bilayer.

DOI: 10.1103/PhysRevB.69.035405 PACS number(s): 68.37.Ps, 68.35.Ct

I. INTRODUCTION

The invention of the scanning tunneling microscope (STM) (Ref. 1) opened the way to microscopy of surfaces with atomic resolution. STM, however, is restricted to conductive samples. Scanning force microscopy (SFM) (Ref. 2) lifts this restriction and enables high-resolution imaging of surfaces regardless of their electric conductivity. The operation of SFM in the dynamic (noncontact) mode offers, in principle, the same resolution as STM. In contrast to STM, SFM involves many different tip-sample interactions, each with a different length scale, resulting in a nonmonotonic tip-sample distance dependence of the interaction. Although both short- and long-range interactions contribute to the measured force, only short-range forces give atomic-scale information. Thus high sensitivity is needed to measure atomic-scale features. Therefore, both experiments and theory are more complex than for STM. For an overview on dynamic SFM see Ref. 3.

An important question for the interpretation of atomically resolved SFM images is how deep SFM senses into the sample. For instance, in the case of the $Si(111)-(7\times7)$ surface, both adatoms and the restatoms below them have been resolved.[4] Combined experimental and theoretical investigations on the CaF_2 (111) surface of cleaved crystals have shown the contribution of several atomic layers to the atomic-scale contrast in SFM images.[5–9] In this paper, we present a SFM study of a CaF bilayer grown on Si(111), where the atomic structure of the two topmost atomic layers is practically identical to the bulk CaF_2 surface[10–13] (cf. Fig. 1). The most significant difference is that F atoms corresponding to the third atomic layer from the surface in bulk CaF_2 are missing in the CaF bilayer. We compare our results with the results published on contrast formation for bulk CaF_2 (111) (Refs. 5–9) to discuss the influence of subsurface features on SFM images.

Additionally, we present a model for atomically resolved SFM on the CaF bilayer based solely on the electrostatic and van der Waals interaction between tip and sample. Although Foster *et al.* have been very successful in quantitatively explaining the details of atomic-scale contrast formation in SFM by using sophisticated simulations,[6,9,32] a simplified, and thus less resource intensive model would be desirable for less detailed interpretation of experimental SFM data. The validity and limitations of the model are discussed by comparing its predictions with our experimental results as well as using results published by others on bulk CaF_2 (111) (Refs. 5–9).

II. EXPERIMENT

CaF_2 is a candidate for the growth of epitaxial insulating films on Si due to its large band gap of 12 eV and its small lattice misfit of 0.6% with respect to Si.[14,15] In contrast to bulk CaF_2 crystals, CaF_2/Si(111) films can be imaged with STM if the thickness of the film does not exceed 1–2 nm.[16] So far, however, only submonolayer CaF_2/Si(111) structures have been imaged with atomic resolution using STM.[16,17] STM seems to be unable to obtain atomic resolution on thicker CaF_2/Si(111) due to the need for relatively high bias voltages. Here, we present atomically resolved images obtained by SFM.

The interface between CaF_2 and Si has been investigated with a wide variety of experimental techniques such as x-ray photoelectron spectroscopy[18,19] and diffraction,[10,11,20] x-ray diffraction,[21,22] medium energy ion scattering,[12] and x-ray

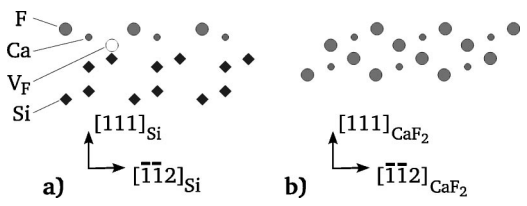

FIG. 1. Atomic structure model of (a) the CaF bilayer on Si with type-B orientation (see text) and Ca atoms on fourfold symmetric tetragonal T_4 sites and (b) bulk CaF_2. V_F denotes the position of the F vacancy. Note the different orientation of the CaF bilayer and the CaF_2 crystal.

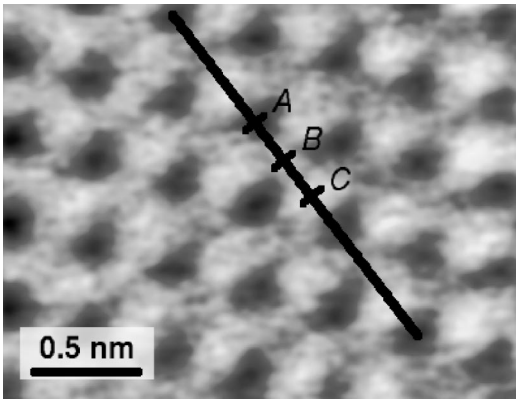

FIG. 2. Atomically resolved SFM image of the CaF bilayer taken at a constant frequency shift of $\Delta f = -800$ Hz and an oscillation amplitude of about 8 nm. The average corrugation is 40 pm. A low-pass filter was applied to the image.[31] The profile along the black line is shown in Fig. 3.

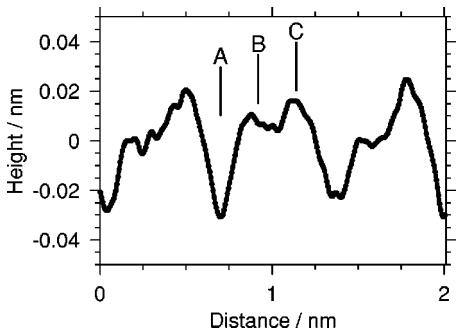

FIG. 3. Single-line profile along the $[11\bar{2}]_{CaF_2}$ direction as marked in Fig. 2. The main features are marked with A, B, and C.

standing waves.[13,23] The most stable configuration of the interface consists of a single nonstoichiometric CaF bilayer (see Fig. 1). CaF_2 grown on top of this bilayer essentially exhibits bulk structural and electronic properties.[15] Both the lattices of the CaF bilayer and the film growing on top of it are rotated by 180° relative to Si around the surface normal (type-B orientation, $[11\bar{2}]_{CaF_2}$ direction points in $[\bar{1}\bar{1}2]_{Si}$ direction, cf. Fig. 1).[24] The formation of the CaF bilayer is driven by the substrate temperature during growth. Complete CaF stoichiometry is obtained for growth temperatures above $\sim 550\,^{\circ}C$.[15]

Si samples were cut from a well-oriented Si(111) wafer and degassed for >12 h at about 600 °C after insertion into ultrahigh vacuum (UHV). The native oxide was removed by flash annealing the samples for 10 s at about 1200 °C. Directly after removal of the oxide, the samples were annealed at 900 °C for 10 min and finally slowly cooled to room temperature. The quality of the Si(111)-(7×7) reconstruction was checked by STM. The CaF_2 films were grown by molecular beam epitaxy (MBE), depositing about 2 TL CaF_2 (one triple-layer [TL] $=7.8\times10^{14}$ CaF_2 molecules/cm^2) at 0.4 TL/min on a Si substrate heated to a temperature of 600 °C. The deposited amount was measured using a quartz microbalance. CaF_2 was sublimed from a pyrolitic boron nitride (PBN) crucible using a Knudsen cell.

SFM measurements were done using a commercial UHV-SFM.[25] SFM images were taken at room temperature in UHV using the frequency modulation technique.[27] The cantilever with a spring constant k of ~ 42 N/m was excited at its resonance frequency f_R of 283 kHz with a constant oscillation amplitude A of about 8 nm. Any interaction between the tip and the sample surface causes a change Δf of f_R. Δf is measured using a digital phase locked loop frequency demodulator[26] and kept constant during image acquisition by regulating the cantilever-sample distance (constant Δf mode). The influence of long-range electrostatic forces between tip and sample was minimized by applying a voltage U between tip and sample. For the particular tip and sample used for Fig. 2, a value of 0.2 V for U was found to minimize $|\Delta f|$ for a fixed cantilever-sample distance.

Under the growth conditions chosen here the Si substrate is completely covered with the CaF bilayer.[15] CaF_2 molecules adsorbing on the CaF bilayer form islands with preferential nucleation at substrate step edges. Sample areas covered with CaF_2 islands can be distinguished from regions with the uncovered CaF bilayer by STM[28,29] or friction force microscopy.[30] Here, we used STM measurements to identify regions covered with the bare CaF bilayer before SFM measurements. These regions covered about 80% of the sample.

III. RESULTS

Figure 2 shows an atomically resolved SFM micrograph of the CaF bilayer with an atomic corrugation of 40 pm. This height variation is much smaller than the 80 pm Ca-F layer spacing and 260 pm Ca-Si layer spacing measured with x-ray standing waves (XSW).[13] The threefold symmetry of the surface can be clearly recognized in the SFM image. Furthermore, the atomic features in the image appear to be triangular shaped. This triangular structure manifests itself in the line profile along one of the high-symmetry directions (see Fig. 3) in the form of shoulders (B) at the main corrugation peaks (C) and dips (A).

The SFM data presented here are strikingly similar to previously published SFM data obtained on cleaved CaF_2 crystals with a positively terminated tip (see below).[5,9] Contrary to our images, the data of Barth *et al.* shown in Refs. 5 and 9 have been obtained in constant height mode. Regions where a large force is measured in constant height mode correspond to regions of high topography in constant frequency shift mode. However, the symmetry of the observed structures is not affected by the measurement mode.

IV. MODEL

Short-range interactions during atomic resolution SFM of ionic crystal surfaces are dominated by electrostatic forces. Therefore, we simulate atomically resolved SFM images of the CaF bilayer taking only contibutions of the short-range electrostatic and long-range van der Waals forces into account. All other forces were neglected.

One major problem for quantitative analysis of SFM data is the unknown microscopic structure and composition of the tip. Good agreement between theory and experiment was ob-

tained for, e.g., bulk CaF_2, by modelling the tip apex with an ionic material cluster.[32] The atomic-scale contrast pattern as predicted by the models and confirmed by experimental results depend on whether the tip is terminated by a positive or negative ion.[5,6,9] We refer to this by discussing our data assuming either a positively or negatively terminated tip.

Density functional theory (DFT) calculations of the electronic structure of the CaF bilayer show that the charge distribution around the Ca and F atoms is similar to bulk CaF_2.[33] The DFT calculations predict a negative net charge above the topmost Si atoms near the position of the F vacancy (V_F) position. Furthermore, core-level energies from photoemission experiments were modeled best by assuming Ca^{2+}, a net charge at V_F, and image charges in the Si substrate.[20] Therefore, we used ionic potentials to model the electrostatic forces between the CaF bilayer and the tip.

Short-range electrostatic forces were calculated using the model of Rotenberg *et al.*[20] assuming a periodic lattice, one molecule thick. A single negative/positive point charge was used to represent a negatively/positively terminated tip. We assumed Ca^{2+} ions and that either one or zero net electron charge is located at the position of the fluorine vacancy (V_F) to study the influence of the missing F ions. The underlying conductive Si was modeled by image charges with an image plane located just below the V_F position. We varied both the magnitude of the Ca-V_F charge transfer and the strength of the image charges. They primarily influence the work function that is compensated by the bias voltage between tip and sample in the experiment but they do not significantly change the predicted corrugation (see Sec. V). Once the electrostatic forces are determined, their contribution Δf_{el} to Δf can be computed using pertubation theory[34,35]

$$\Delta f_{el} = \frac{f_0}{2\pi kA} \int_0^{2\pi} d\phi F_{el}[z_0 + A\cos(\phi)]\cos(\phi), \qquad (1)$$

where $F_{el}(z)$ denotes the electrostatic force with the time-dependent position of the tip given by $z = z_0 + A\cos(2\pi ft)$.

The van der Waals force was modeled assuming a conical tip shape terminated by a sphere with radius R using the following equation for the dependence of the frequency shift on the closest approach tip-sample distance:[35]

$$\Delta f_{vdW}(z) = -\frac{f_0 HR}{12\sqrt{2}kA^{3/2}} z^{-3/2} \qquad (2)$$

with the cantilevers spring constant k, free resonance frequency f_0, and Hamaker constant H. We chose a value of 4×10^{-19} J for the Hamaker constant of the tip/sample system.[35] To estimate the van der Waals forces during our experiments, we measured the dependence of Δf on z. Figure 4 shows the experimental data for $\Delta f(z)$ as well as a fit of Eq. (2) to the part of the data that should be dominated by the long-range van der Waals force. The least-squares fit resulted in a value of 80 nm for the tip radius.

The frequency shift Δf was computed by the addition of the van der Waals and electrostatic contributions: $\Delta f = \Delta f_{vdW} + \Delta f_{el}$.[35]

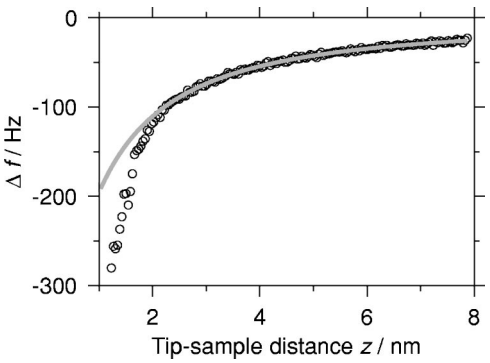

FIG. 4. Dependence of the frequency shift Δf on the tip-sample distance z. The circles show the experimental data. The gray curve shows a fit of Eq. (2) to this data for $z \geqslant 3$ nm. (The zero point of z is chosen arbitrarily.)

Simulations of SFM have shown that the tip and sample atoms involved in the formation of atomic scale contrast are not static but move from their original positions in the crystal lattice under the influence of the forces between tip and sample.[6,36] The theoretical work of Foster *et al.* shows that the magnitude of the atomic relaxations caused by the tip-sample interactions is up to few 10 pm for the case of bulk CaF_2.[6] This is in the same range as the atomic corrugations observed by us for imaging the CaF bilayer. Therefore, tip induced deformations cannot be neglected in the discussion of atomic-scale contrast interpretation.

To estimate the influence of the tip-induced deformations of the sample we modify the positions of the ions in our periodic lattice and compute the electrostatic force for the modified setup. In contrast to the more complex simulations by Foster *et al.*[6] our simplified approach is static: the positions of the ions do not change with the tip position.

V. DISCUSSION

As already stressed in Sec. III, the SFM data of the CaF bilayer shown in Figs. 2 and 3 is very similar to SFM data obtained for positive tip termination on bulk CaF_2 published by Barth *et al.*[5,9] The fact that the F layer at the interface is vacant seems to have no influence on the contrast in atomically resolved SFM images. The three high-symmetry points (A,B,C) of the image shown in Fig. 2 can be assigned to the symmetry points of the CaF bilayer that are the positions of the F atom, Ca atom, and the vacancy position (V_F) above the topmost Si atom (see Fig. 1). The symmetry and crystallographic orientation restrict the assignment of the positions (A,B,C) to the three following combinations: (Ca, V_F, F), (F, Ca, V_F), and (V_F, F, Ca).

Figure 5 shows simulated linescans along the $[11\bar{2}]_{CaF_2}$ direction. The general shape of the simulated linescans is similar to the experimental data shown in Fig. 3. Imaging with a negatively terminated tip results in corrugation maxima above cations while imaging with a positively terminated tip produces images with maxima above anions. A comparison between the measured and simulated linecan (compare Figs. 3 and 5) yields that our data agree only with

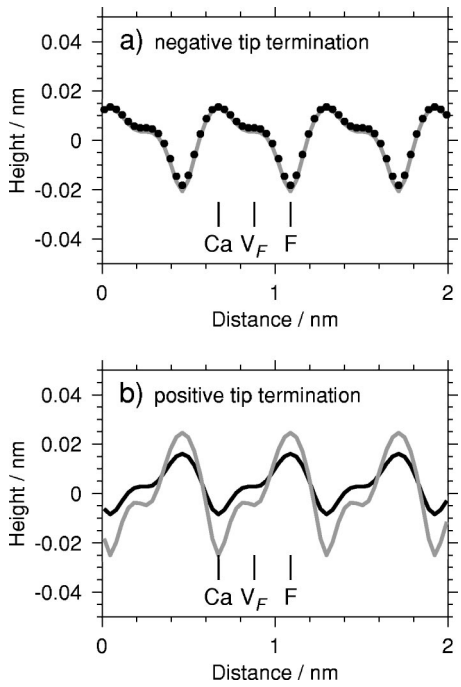

FIG. 5. Simulated line profiles with a constant Δf of -390 Hz (see text) along the $[11\bar{2}]_{CaF_2}$ direction for negatively [(a) top] and positively terminated tips [(b) bottom]. Both linescans shown in (a) were computed with image charges in place, and static deformations moving the Ca cations upwards and F anions down (into the sample). For the solid (dotted) line in (a) the charge located at V_F was set to $-e$ (zero). The linescans for the positive tip termination shown in (b) were computed without image charges and with nominal Ca^{2+} ions and one electron located at V_F. The gray line assumed static sample deformations moving Ca cations downwards and F anions upwards while the black line shows a calculation for bulk CaF_2 coordinates.

the simulation results for a positively terminated tip. Therefore, the positions (A,B,C) (cf. Fig. 2) would be assigned to (Ca, V_F, F). For the following discussion we assume that our tip had a net positive electrostatic potential.

The model introduced in Sec. IV predicts that atomic resolution can only be obtained within a 20 Hz wide range of Δf. For higher $|\Delta f|$ imaging with constant Δf is predicted to become unstable due to the nonmonotonous behavior of $\Delta f(z)$ while smaller values do not result in a sufficient corrugation. However, atomic resolution images were acquired with frequency shifts between -600–-800 Hz. This broad range of experimental values for Δf may be explained by multiple tip changes that occured during the experiments presented here. Nevertheless, the maximum corrugation of about 40 pm predicted by the model agrees remarkably well with the experimental observations.

Figure 5(a) shows SFM linescans simulated using identical parameters except for different charges located at V_F. Both linescans are identical and additional calculations showed that the charge at V_F apparantly has no influence on the atomic corrugation and changes only the workfunction. Therefore, SFM images of the CaF bilayer and bulk CaF_2 should be very similar regardless of the amount of charge present at V_F. It should be noted that the influence of the charge located at V_F on the atomic corrugation becomes significant for smaller tip-sample distances. As noted above, scanning with constant Δf in these distances, however, is predicted to be unstable. Microscopy techniques sensitive to work function changes such as Kelvin probe microscopy may be able to image areas with and without the F vacancies below the Ca layer as observed for lower growth temperatures by, e.g., XSW.[13]

This opens the question why the simulated SFM linescans show a shoulder at V_F which is independent of the charge present at V_F, even though we take only electrostatic forces into account. This may be understood by considering that on ionic surfaces long-range contributions to the Madelung potential are very important to the local electrostatic potential. For instance, taking only the seven nearest neighbors into account leads even to a wrong sign for the electrostatic potential.

The influence of static deformations of the atomic lattice is demonstrated in Fig. 5(b) showing SFM linescans simulated with parameters differing only in the location of the ions in the periodic lattice comparing the linescan obtained using bulk CaF_2 coordinates that are practically identical to the CaF bilayer structure[37] with a linescan simulated for a lattice deformed by the tip-sample interaction. As the static model described in Sec. IV cannot predict the complex motion of the sample's ions below the oscillating tip, we used the maximum deformation amplitude calculated by the more advanced simulations of SFM on bulk CaF_2 by Foster *et al.*[6] to estimate the amount of lattice deformation. Within the limitations of our static model, tip induced sample deformations increase the corrugation amplitude but leave the overall shape of the linescans unchanged. While the former is consistent with the predictions of Foster *et al.*,[32] their atomistic simulations show a more drastic influence of the sample (and tip) deformations as discussed below.

Figure 2 shows that the atomically resolved images of the CaF bilayer consist of a triangular pattern. This is consistent with previously published results obtained by combined theoretical and experimentical studies for the case of images obtained with a positively terminated tip.[5,9,32] However, we did not observe the circular contrast pattern attributed to negatively terminated tips that is both theoretically predicted and experimentally observed for the bulk CaF_2 (111) surface.[5,9,32] This can be explained by in two ways: Firstly, our data was obtained using only one tip that may have been positively terminated during all experiments. Secondly, the circular contrast pattern is caused by the dynamics of the tip-induced atomic deformations (see below).[5] These deformations may be different for the CaF bilayer than for bulk CaF_2. Further experimental and theoretical studies are required to clarify the details of atomic-scale contrast formation on the CaF bilayer.

Our simplified SFM model predicts a triangular contrast pattern for both positive and negative tip terminations. In the case of imaging bulk CaF_2 with a negatively terminated tip the Ca cations are pulled out of the surface upon each approach of the tip while the F anions are pushed into the sample. The combination of these relaxations causes a domination of the tip-sample interaction by the Ca cations result-

ing in the circular contrast pattern that cannot be explained without taking these deformations into account.[5] Even though our model includes tip-induced sample deformations by assuming a static deformation of the atomic lattice, it is not able to predict the circular contrast pattern caused by dynamic relaxations and thus predicts the same contrast pattern for both tip terminations.

VI. CONCLUSIONS

In conclusion, we presented atomically resolved SFM images of the CaF bilayer on Si(111). Our images are very similar to SFM data on the bulk CaF_2 (111) surface obtained with a tip with positive termination.[5,6,9] The difference between the geometric structure of bulk CaF_2 and the CaF bilayer grown on Si(111) in the third layer from the surface seems to have no influence on the SFM images reported here.

We presented a simple model based on electrostatic and van der Waals interactions between tip and sample. On one hand, the model fails when dynamic processes such as tip induced sample relaxations become the most important factor in contrast formation as it is the case of the circular contrast pattern for SFM imaging of bulk CaF_2 with a negatively terminated tip.[5,6,9] On the other hand, the model allowed us to allocate the symmetry points in atomically resolved SFM images of the CaF bilayer to atomic positions and correctly predicts the atomic corrugation amplitude. Furthermore, the model predicts that the atomic-scale contrast on the CaF bilayer is not sensitive to the amount of charge located at the F vacancy position between Ca and Si (V_F) due to the strong contributions of long-range interactions on the surface Madelung potential explaining the similarity of the data on the CaF bilayer with data obtained on bulk CaF_2.[5,6,9]

ACKNOWLEDGMENTS

The authors gratefully acknowledge stimulating discussions with R. Hoffmann and S. Fain. This work is supported by the U.S. Department of Energy Grant No. DE-FG03-97ER45646 and the M. J. Murdock Charitable Trust. A.K. further acknowledges support by the Alexander von Humboldt-Foundation and T.O. acknowledges financial support from the University Initiative Fund of the University of Washington.

*Present address: Department of Physics, Tulane University, New Orleans, LA 70118. Electronic address: aklust@tulane.edu

[1] G. Binnig, H. Rohrer, C. Gerber, and E. Weibel, Phys. Rev. Lett. **49**, 57 (1982).
[2] G. Binnig, C.F. Quate, and C. Gerber, Phys. Rev. Lett. **56**, 930 (1986).
[3] *Noncontact Atomic Force Microscopy*, edited by S. Morita, R. Wiesendanger, and E. Meyer (Springer, New York, 2002).
[4] M.A. Lantz, H.J. Hug, P.J.A. van Schendel, R. Hoffmann, S. Martin, A. Baratoff, A. Abdurixit, H.-J. Güntherodt, and C. Gerber, Phys. Rev. Lett. **84**, 2642 (2000).
[5] A.S. Foster, C. Barth, A.L. Shluger, and M. Reichling, Phys. Rev. Lett. **86**, 2373 (2001).
[6] A.S. Foster, A.L. Shluger, and R.M. Nieminen, Appl. Surf. Sci. **188**, 306 (2002).
[7] M. Reichling and C. Barth, Phys. Rev. Lett. **83**, 768 (1999).
[8] C. Barth and M. Reichling, Surf. Sci. **470**, L99 (2000).
[9] C. Barth, A.S. Foster, M. Reichling, and A.L. Shluger, J. Phys.: Condens. Matter **13**, 2061 (2001).
[10] J.D. Denlinger, E. Rotenberg, U. Hessinger, M. Leskovar, and M.A. Olmstead, Appl. Phys. Lett. **62**, 2057 (1993).
[11] J.D. Denlinger, E. Rotenberg, U. Hessinger, M. Leskovar, and M.A. Olmstead, Phys. Rev. B **51**, 5352 (1995).
[12] R.M. Tromp and M.C. Reuter, Phys. Rev. Lett. **61**, 1756 (1988).
[13] A. Klust, M. Bierkandt, J. Wollschläger, B.H. Müller, T. Schmidt, and J. Falta, Phys. Rev. B **65**, 193404 (2002).
[14] L.J. Schowalter and R.W. Fathauer, CRC Crit. Rev. Solid State Mater. Sci. **15**, 367 (1989).
[15] M.A. Olmstead, *Thin Films: Heteroepitaxial Systems* (World Scientific, Singapore, 1999), Chap. 5, pp. 211–266.
[16] P. Avouris and R. Wolkow, Appl. Phys. Lett. **55**, 1074 (1989).
[17] T. Sumiya, T. Miura, and S. Tanaka, Surf. Sci. **357-358**, 896 (1996).
[18] F.J. Himpsel, U.O. Karlsson, J.F. Morar, D. Rieger, and J.A. Yarmoff, Phys. Rev. Lett. **56**, 1497 (1986).
[19] M.A. Olmstead, R.I.G. Uhrberg, R.D. Bringans, and R.Z. Bachrach, Phys. Rev. B **35**, 7526 (1987).
[20] E. Rotenberg, J.D. Denlinger, M. Leskovar, U. Hessinger, and M.A. Olmstead, Phys. Rev. B **50**, 11 052 (1994).
[21] C.A. Lucas, D. Loretto, and G.C.L. Wong, Phys. Rev. B **50**, 14 340 (1994).
[22] K.G. Huang, J. Zegenhagen, J.M. Phillips, and J.R. Patel, Phys. Rev. Lett. **72**, 2430 (1994).
[23] J. Zegenhagen and J.R. Patel, Phys. Rev. B **41**, 5315 (1990).
[24] H. Ishiwara and T. Asano, Appl. Phys. Lett. **40**, 66 (1982).
[25] Omicron Nanotechnology GmbH, Taunusstein, Germany.
[26] Easy PLL Digital FM-Detector, Nanosurf AG, Liestal, Switzerland.
[27] T.R. Albrecht, P. Grütter, D. Horne, and D. Rugar, J. Appl. Phys. **69**, 668 (1991).
[28] J. Viernow, D.Y. Petrovykh, A. Kirakosian, J.-L. Lin, F.K. Men, M. Henzler, and F.J. Himpsel, Phys. Rev. B **59**, 10 356 (1999).
[29] M. Bierkandt, Ph.D. thesis, Universität Hannover, 2003.
[30] A. Klust, H. Pietsch, and J. Wollschläger, Appl. Phys. Lett. **73**, 1967 (1998).
[31] P. Zahl, M. Bierkandt, S. Schröder, and A. Klust, Rev. Sci. Instrum. **74**, 1222 (2003).
[32] A.S. Foster, C. Barth, A.L. Shluger, R.M. Nieminen, and M. Reichling, Phys. Rev. B **66**, 235417 (2002).
[33] M.R. Salehpour, S. Satpathy, and G.P. Das, Phys. Rev. B **44**, 8880 (1991).
[34] F.J. Giessibl, Phys. Rev. B **56**, 16 010 (1997).
[35] M. Guggisberg, M. Bammerlin, C. Loppacher, O. Pfeiffer, A. Abdurixit, V. Barwich, R. Bennewitz, A. Baratoff, E. Meyer, and H.-J. Güntherodt, Phys. Rev. B **61**, 11 151 (2000).
[36] N. Sasaki, S. Watanabe, and M. Tsukada, Phys. Rev. Lett. **88**, 046106 (2002).
[37] A. Klust, R. Kayser, and J. Wollschläger, Phys. Rev. B **62**, 2158 (2000).